Non-Hermitian higher-order topological insulators enabled by altermagnet engineering

Xiang Ji [1,2,3] Dengfeng Wang,[1] Tong Zhou,[2,*] and Xiaosen Yang [1,†]

[1]*Department of Physics, Jiangsu University, Zhenjiang 212013, China*

[2]*Eastern Institute for Advanced Study, Eastern Institute of Technology, Ningbo, Zhejiang 315200, China*

[3]*School of Physics and Astronomy, Shanghai Jiao Tong University, Shanghai 200240, China*

(Received 31 December 2025; revised 19 May 2026; accepted 8 June 2026; published 18 June 2026)

We show that proximity to an altermagnet provides an efficient route to engineering non-Hermitian higher-order topological phases. The proximity-induced altermagnetic order gaps the edge states of a topological insulator, thereby driving a transition from a first-order to a second-order topological phase. When combined with nonreciprocal hopping, the system exhibits both the non-Hermitian skin effect and a hybrid skin-topological effect, whereby first-order edge states and second-order corner states accumulate at selected corners of the lattice. We demonstrate that the spectral winding number of the edge states under cylindrical geometry dictates this corner localization and can be reversed by tuning the altermagnetic order. Consequently, both edge and corner states become directionally controllable. Our results establish altermagnets as a versatile platform for realizing and tuning skin-topological phenomena in non-Hermitian higher-order topological systems.

DOI: 10.1103/xbzb-jgk9

I. INTRODUCTION

Altermagnetism has recently emerged as a distinct class of collinear magnetic order that bridges the physics of ferromagnets and antiferromagnets [1–14]. It exhibits large momentum-dependent spin polarization while maintaining zero net magnetization, thus realizing time-reversal-odd spin splitting with compensated magnetic moments [12,14]. This unique symmetry realization enriches the taxonomy of magnetic phases and provides an intrinsic route to dissipationless spin control without stray fields. Its symmetry-filtered spin texture enables precise band-structure engineering, as verified theoretically and experimentally in MnTe [15–17], CrSb [18–20], Mn_5Si_3 [21,22], RbV_2Se_2O [14], and KV_2Se_2O [23,24]. Due to its time-reversal breaking band structure and alternating momentum-dependent spin splitting, altermagnetism gives rise to a variety of novel effects and phases, including the crystal Hall effect [3,25–27], giant tunneling magnetoresistance [28,29], spin-momentum interactions [30–32], unique proximity effect [33,34], and topological phases [35–40].

In recent years, the study of topological phases has been extended to non-Hermitian systems, attracting substantial research interest [41–62]. Non-Hermitian systems exhibit a variety of striking phenomena that have no counterpart in Hermitian physics [63–68]. Among the most prominent are exceptional points [69,70], where both eigenvalues and eigenvectors coalesce, and the non-Hermitian skin effect (NHSE) [45,71–81], which drives an extensive number of bulk states to accumulate at system boundaries under open boundary conditions (OBCs). By reshaping the topology of complex energy spectra, non-Hermiticity enables unconventional topological phenomena, especially in higher dimensions. In particular, the hybridization of topological edge states with the NHSE gives rise to the skin-topological effect, where topologically protected edge states localize directionally at lower-dimensional boundaries [82–92]. These phenomena highlight the importance of understanding how non-Hermiticity interacts with intrinsic topological boundary states. The absence of stray magnetic fields makes altermagnets especially appealing for realizing non-Hermitian phenomena, since external magnetic fields may suppress or obscure the NHSE [93,94]. While recent works have examined exceptional-point physics in non-Hermitian altermagnets [95,96], the NHSE and its coupling to higher-order topology in altermagnetic platforms remain largely unexplored.

In this work, we demonstrate that proximitizing an altermagnet to a non-Hermitian topological insulator provides an effective and controllable route to engineering non-Hermitian higher-order topological phases. Altermagnetism opens a gap in the topological edge states of the topological insulator, leading to a topological phase transition from a first-order topological phase to a second-order topological phase. When combined with nonreciprocal hopping, the system exhibits both the NHSE and the hybrid skin-topological effect. The latter, manifested as the accumulation of first-order edge states at the corners of the system, is dictated by the spectral winding number of the edge bands under cylindrical geometry. Crucially, the proximitized altermagnetic order serves as a powerful tuning knob: by modifying the band dispersion of the edge states, it reverses the spectral winding number and thereby switches the localization direction of the topological edge states. As the topological corner states inherit this skin-topological effect, they likewise accumulate at tunable corners of the lattice. These results establish altermagnetism as a versatile mechanism for designing and controlling non-Hermitian higher-order topological phases.

*Contact author: tzhou@eitech.edu.cn

†Contact author: yangxs@ujs.edu.cn

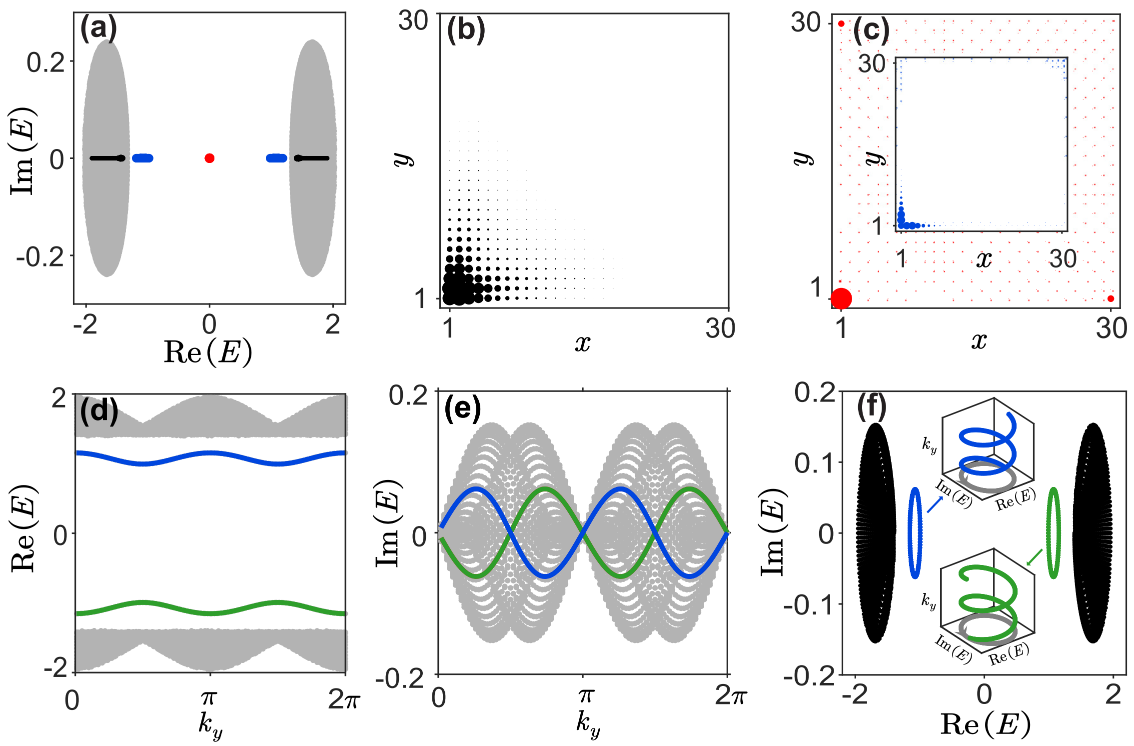

FIG. 1. Energy spectrum and spatial distributions in the presence of strong altermagnetism. (a) Energy spectrum for a 30 × 30 square lattice under PBC (gray) and OBC (other points), respectively. The black, blue, and red dots represent the energies of bulk states, first-order edge states, and second-order corner states, respectively. (b) Average probability distributions of bulk states under OBC. (c) Probability distributions of second-order corner states. The inset shows the average probability distributions of first-order edge states. (d) and (e) Real and imaginary parts of the energies as a function of k_y for the system under OBC_x–PBC_y. (f) Complex energy spectrum of the system under OBC_x–PBC_y. The insets show the spectral winding of edge states. In panels (d)–(f), edge states with positive (negative) real parts of the energy are indicated by blue (green) markers. Parameters: $t_x = t_y = A_x = A_y = 1$, $\delta_x = \delta_y = 0.2$, $J = 0.7$, and $m_0 = 0$.

II. SWITCHABLE SKIN-TOPOLOGICAL EFFECT

We consider a two-dimensional non-Hermitian insulator in proximity to a $d_{x^2-y^2}$-wave altermagnet, whose Bloch Hamiltonian is given by

$$H(\mathbf{k}) = H_{\mathrm{TI}}(\mathbf{k}) + H_{\mathrm{NH}}(\mathbf{k}) + H_{\mathrm{AM}}(\mathbf{k}). \tag{1}$$

Here, $H_{\mathrm{TI}}(\mathbf{k}) = (m_0 - t_x \cos k_x - t_y \cos k_y)\sigma_x + A_x \sin k_x \sigma_z s_x + A_y \sin k_y \sigma_z s_y$ describes a Hermitian topological insulator that preserves time-reversal symmetry and hosts helical edge states, relevant to materials like HgTe and WTe_2 [97–99]. The non-Hermiticity is introduced by $H_{\mathrm{NH}}(\mathbf{k}) = (-i\delta_x \sin k_x - i\delta_y \sin k_y)\sigma_x$, which effectively describes nonreciprocal hopping generated by an imaginary gauge field, where the hopping amplitudes along the positive and negative x and y directions acquire asymmetric Peierls factors [95,100].

The proximity-induced altermagnetic order [33,36], which can be supported by realistic altermagnetic materials, is described by

$$H_{\mathrm{AM}}(\mathbf{k}) = J(\cos k_x - \cos k_y)\sigma_z s_z, \tag{2}$$

where J denotes the effective altermagnetic strength and can be tuned by varying the layer spacing [33,36]. s_i and σ_i denote the Pauli matrices acting on spin and orbital degrees of freedom, respectively.

In the absence of altermagnetism ($J = 0$), the Hamiltonian reduces to a non-Hermitian topological insulator hosting gapless helical edge states that are evenly localized at four edges of the lattice. Turning on the altermagnetic order fundamentally restructures the phase diagram and drives the system into a higher-order topological phase. To elucidate the physical mechanism, we initially focus on the $m_0 = 0$ case. In particular, we show the energy spectrum of the system with $J = 0.7$ in Fig. 1(a), where the spectrum under periodic boundary conditions (PBCs) appears in gray, while the OBC spectrum is separated into three parts corresponding to bulk states (black), first-order edge states (blue), and second-order corner states (red).

The altermagnetic order gaps the helical edge states, generating four in-gap corner states and driving the system into a second-order topological insulator. The nonreciprocal hopping renders the spectrum highly sensitive to the boundary conditions: relative to the PBC bands, the OBC bulk energies undergo a pronounced collapse, signaling the NHSE. The spatial distribution in Fig. 1(b) confirms that the bulk states accumulate at the lower-left corner of the square lattice, consistent with the direction of nonreciprocal pumping. Beyond the NHSE of the bulk states, the interplay between altermagnetism and non-Hermiticity also reshapes the localization of topological edge states. As shown in the inset of Fig. 1(c), altermagnetic order and non-Hermiticity drive the first-order edge states to accumulate at the lower-left corner of the lattice, a hallmark of the skin-topological effect, in sharp contrast to the $J = 0$ case where the edge states remain uniformly distributed along the boundaries. The skin-topological effect further influences the second-order corner states: as illustrated in Fig. 1(c), the in-gap zero states preferentially localize at the lower-left corner, rather than appearing symmetrically at all four corners as in the Hermitian limit or absence of altermagnetism.

To gain a deeper understanding of the skin-topological states, we analyze the spectral winding number of the edge states under a cylindrical geometry. While the point-gap topology is the standard diagnostic of the NHSE in one-dimensional non-Hermitian systems [74,75], here we use the spectral winding number of edge states under cylindrical geometry to characterize the skin-topological effect. Figures 1(d) and 1(e) show the real and imaginary parts of the spectrum for the OBC along the x direction and the PBC along the y direction (OBC_x–PBC_y), respectively. As the edge states under this cylindrical geometry disperse both in their real and imaginary parts, their trajectories in the complex-energy plane form a point gap, as illustrated in the insets of Fig. 1(f). Since the edge-state branches are separated from the bulk branches in the k_y-resolved spectrum, the corresponding edge-state spectral winding number with respect to a reference energy E can be defined as

$$\mathcal{W}_{\mathrm{edge}}(E) = \sum_{n\in\mathrm{edge}} \int_0^{2\pi} \frac{dk_y}{2\pi i} \partial_{k_y} \log\left[E_n^{\mathrm{edge}}(k_y) - E\right], \quad (3)$$

where $E_n^{\mathrm{edge}}(k_y)$ denotes the energies of nth edge states under cylindrical geometry. Here, we take counterclockwise encircling in the complex-energy plane as the positive orientation. A positive/negative edge winding indicates that, when the y direction is further opened, the corresponding edge modes accumulate toward the lower/upper end of the lattice. Moreover, for the symmetric parameter set used here, the spectra under the OBC_x–PBC_y and PBC_x–OBC_y geometries are equivalent. Therefore, with the convention adopted in the paper, a positive/negative edge winding under the cylindrical geometry is associated with the accumulation of edge states toward the lower-left/upper-right corner under full OBC. The complex energies of the edge states under OBC_x–PBC_y are shown in Fig. 1(f). We find that the spectral winding number is positive, indicating that the first-order edge states under full OBC accumulate at the lower-left corner of the lattice. Notably, reversing the direction of nonreciprocal pumping, e.g., ($\delta \to -\delta$), reverses the imaginary dispersion and changes the winding number to be negative, causing the first-order edge states to accumulate at the upper-right corner. Since the second-order corner states originate from the altermagnetic-order-induced gapping of the topological edge modes, their wave functions are affected by the directional skin accumulation of the parent edge-state subspace. This explains why the corner states localize at the same selected corners as the skin-topological edge modes.

Furthermore, varying the altermagnetic strength J significantly modifies the real part of the edge-state dispersion under cylindrical geometry. The localization behavior of the skin-topological states and second-order corner states changes when a relatively small J is applied. To illustrate this, we show the real and imaginary energies of the system under cylindrical geometry with $J = 0.3$ as a function of k_y in Figs. 2(a) and 2(b), respectively. The energies whose real parts are positive (negative) and closest to zero are marked in blue (green). The sign of the real dispersion is opposite to the strong altermagnetism case in Fig. 1(d), while the signs of the imaginary dispersion remain the same. Therefore, the spectral winding numbers under cylindrical geometry are reversed compared to the case of $J = 0.7$. As shown in Fig. 2(c), the spectral winding numbers become negative, indicating that the first-order edge states will accumulate at the upper-right corner of the lattice, which is opposite to the strong altermagnetism case. Affected by the skin-topological effect, although the bulk states localize at the lower-left corners of the system, the corner states tend to appear at the same corner as the first-order edge states and do not appear at the lower-left corner, as shown in Fig. 2(d).

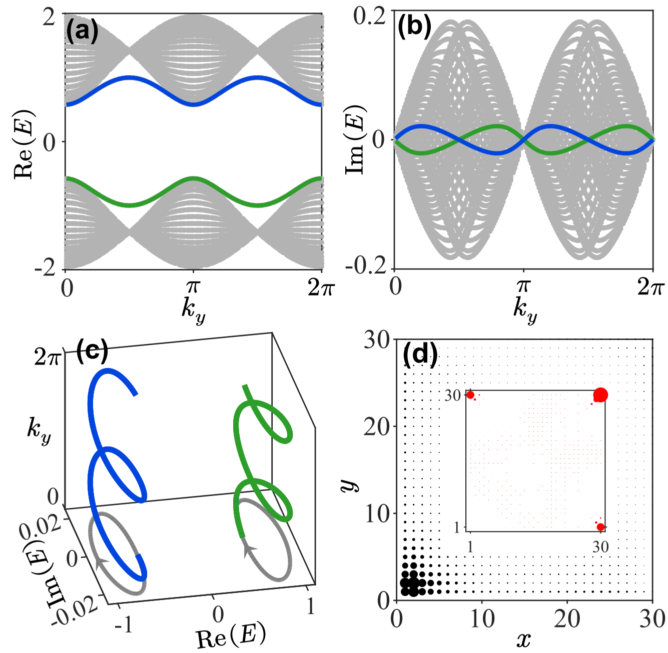

FIG. 2. Weak altermagnetism case ($J = 0.3$). (a) and (b) Real and imaginary parts of the energies as functions of k_y for the system under cylindrical geometry. Topological edge states with positive (negative) real parts of the energy are marked in blue (green). (c) Complex energy spectrum of the edge states as a function of k_y. Edge states in panels (a)–(c) are color coded blue and green to indicate positive and negative real parts of the energy, respectively. (d) Average probability distributions of bulk states under OBC. Inset: average probability distribution of zero states.

Overall, the skin-topological states and second-order corner states are localized at the opposite corners of the lattice when we apply different strengths of altermagnetism, which can be well explained by the spectral winding number of the edge states under cylindrical geometry. Therefore, tuning the strength of the altermagnetism provides a feasible method to tune the localization behavior of the topological states.

III. EDGE FLAT BANDS AND BIPOLAR SKIN-TOPOLOGICAL EFFECT

We have shown that both the skin-topological states and second-order corner states can be switched by tuning the

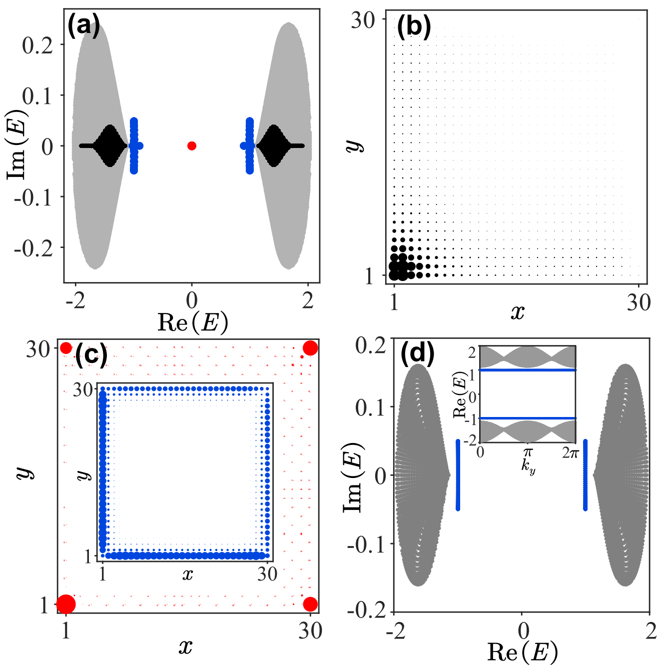

FIG. 3. The critical point at $J = 0.57$. (a) Complex energy spectrum. (b) Average probability distribution of the bulk states. (c) Average probability distribution of the corner states and first-order edge states (inset) of the system under OBC. (d) The complex spectrum of the system under OBC_x–PBC_y. The inset shows the real parts of energies as functions of k_y.

altermagnetic order, implying the existence of a critical altermagnetic strength $J_c = 0.57$ between the weak and strong regimes. To illustrate this transition, we present the energy spectrum and probability distribution of the bulk states in Figs. 3(a) and 3(b), respectively. In this case, the system remains in a higher-order topological phase and hosts four in-gap zero states while the bulk states under OBC accumulate at the lower-left corners of the lattice due to the nonreciprocal hopping. The first-order edge states are uniformly distributed along all four edges, as shown in the inset of Fig. 3(c), indicating the absence of the skin-topological effect. The second-order corner states also appear symmetrically at all four corners without any directional preference. This absence of both edge localization and corner selectivity originates from the flat real energy dispersion of the edge states under cylindrical geometry, as depicted in Fig. 3(d), which results in a zero spectral winding number and suppresses the skin-topological effect.

Although our analysis primarily focuses on the $m_0 = 0$ case, the underlying control mechanism remains robust for finite m_0, demonstrating the physical universality of the observed phenomena across a broader parameter regime. When a finite m_0 is introduced, the winding behavior of the edge states under cylindrical geometry becomes more intricate, and a bipolar skin-topological effect can emerge near the transition point discussed above. As an illustrative example, we take $m_0 = 0.2$ and $J = 0.57$, and plot the spectrum of the first-order edge states in Fig. 4(a). In this case, the energies obtained under full OBC and cylindrical geometry are shown as colored and gray points, respectively. These energies are

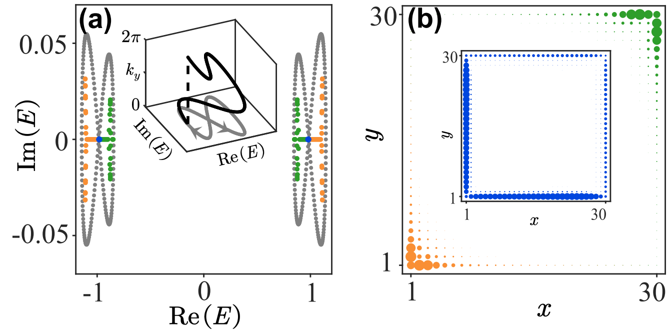

FIG. 4. The bipolar skin-topological effect. (a) The gray points depict the energies of the edge states under OBC_x–PBC_y, while colored points represent the energies under full OBC with $m_0 = 0.2$. The inset shows the complex spectrum under cylindrical geometry as a function of k_y. (b) Average probability distribution of the edge states under full OBC, with colors corresponding to the energies highlighted in (a).

spectrally isolated from the bulk continuum. The edge states under full OBC with positive and negative spectral winding numbers, as extracted from the inset, are marked in orange and green, respectively. When the system is opened in both directions, the edge branches with opposite winding numbers will accumulate at opposite ends of the boundary, i.e., at opposite corners of the two-dimensional sample, leading to the bipolar skin-topological effect. As shown in Fig. 4(b), these states localize at opposite corners of the lattice, with the probability distributions color matched to the corresponding points in Fig. 4(a). Remarkably, the states at the intersections between regions of opposite winding numbers correspond to Bloch-edge states, marked by blue points in Fig. 4(a). These states are extended along the edges rather than localized at the corners, as confirmed in the inset of Fig. 4(b).

IV. CONCLUSION

In this work, we have investigated the non-Hermitian second-order topological insulator realized by placing a non-Hermitian topological insulator in proximity to an altermagnet. The nonreciprocal hopping drives the bulk states to accumulate at the lattice corners, generating a pronounced non-Hermitian skin effect. Meanwhile, the altermagnetic order gaps the topological edge states and induces a transition from a first-order to a second-order topological phase. The interplay between altermagnetism and non-Hermiticity produces a skin-topological effect, in which the first-order edge states are driven to the corners of the lattice. This effect is accurately captured by the spectral winding number of the edge states under cylindrical geometry. Crucially, the proximitized altermagnetic order reshapes the real-part edge dispersion, enabling a sign reversal of the spectral winding number and thus a controllable inversion of edge and corner localization, without altering the direction of nonreciprocal hopping. As a consequence, the second-order corner states inherit the skin-topological localization and preferentially accumulate at the same corners as the edge states. Our results reveal the rich interplay between altermagnetism and non-Hermiticity, demonstrating that non-Hermitian altermagnets offer a versatile and tunable platform for manipulating topological edge and corner states.

The nonreciprocal hopping in our model can be readily implemented in cold-atom platforms using Raman-assisted schemes and programmable lattices [101], acoustics [102], topological circuits [103], and optics [53]. In electronic settings, nonreciprocal hopping may be effectively engineered via bilayer or multiorbital coupling [104–106]. The altermagnetic order in our model can be realized in heterostructures by interfacing a two-dimensional topological insulator with a layered altermagnet [33,36], in which the effective altermagnetic strength can be tuned by varying the interlayer distance. The predicted switchable hybrid skin-topological effect and second-order corner modes may be probed in electronic realizations by scanning tunneling microscopy/spectroscopy through spatial mapping of the local density of states [107,108]. Notably, although we characterize the skin-topological effect using the spectral winding number under cylindrical geometry, a comprehensive understanding of such effects across different dimensions and symmetry classes remains to be developed. Furthermore, the interaction between skin-topological states and higher-order topological states represents an open question that merits further exploration.

ACKNOWLEDGMENTS

This work was supported by Natural Science Foundation of Jiangsu Province (Grant No. BK20231320), National Natural Science Foundation of China (Grant No. 12474155), and the Zhejiang Provincial Natural Science Foundation of China (Grant No. LR25A040001).

DATA AVAILABILITY

The data that support the findings of this article are not publicly available. The data are available from the authors upon reasonable request.

[1] S. Hayami, Y. Yanagi, and H. Kusunose, Momentum-dependent spin splitting by collinear antiferromagnetic ordering, J. Phys. Soc. Jpn. **88**, 123702 (2019).

[2] L.-D. Yuan, Z. Wang, J.-W. Luo, E. I. Rashba, and A. Zunger, Giant momentum-dependent spin splitting in centrosymmetric low-z antiferromagnets, Phys. Rev. B **102**, 014422 (2020).

[3] Libor Šmejkal, R. González-Hernández, T. Jungwirth, and J. Sinova, Crystal time-reversal symmetry breaking and spontaneous Hall effect in collinear antiferromagnets, Sci. Adv. **6**, eaaz8809 (2020).

[4] Libor Šmejkal, J. Sinova, and T. Jungwirth, Beyond conventional ferromagnetism and antiferromagnetism: A phase with nonrelativistic spin and crystal rotation symmetry, Phys. Rev. X **12**, 031042 (2022).

[5] Libor Šmejkal, J. Sinova, and T. Jungwirth, Emerging research landscape of altermagnetism, Phys. Rev. X **12**, 040501 (2022).

[6] L. Bai, W. Feng, S. Liu, L. Šmejkal, Y. Mokrousov, and Y. Yao, Altermagnetism: Exploring new frontiers in magnetism and spintronics, Adv. Funct. Mater. **34**, 2409327 (2024).

[7] C. Song, H. Bai, Z. Zhou, L. Han, H. Reichlova, J. H. Dil, J. Liu, X. Chen, and F. Pan, Altermagnets as a new class of functional materials, Nat. Rev. Mater. **10**, 473 (2025).

[8] Y. Jiang, Z. Song, T. Zhu, Z. Fang, H. Weng, Z.-X. Liu, J. Yang, and C. Fang, Enumeration of spin-space groups: Towards a complete description of symmetries of magnetic orders, Phys. Rev. X **14**, 031039 (2024).

[9] X. Chen, J. Ren, Y. Zhu, Y. Yu, A. Zhang, P. Liu, J. Li, Y. Liu, C. Li, and Q. Liu, Enumeration and representation theory of spin space groups, Phys. Rev. X **14**, 031038 (2024).

[10] Z. Xiao, J. Zhao, Y. Li, R. Shindou, and Z.-D. Song, Spin space groups: Full classification and applications, Phys. Rev. X **14**, 031037 (2024).

[11] P. A. McClarty and J. G. Rau, Landau theory of altermagnetism, Phys. Rev. Lett. **132**, 176702 (2024).

[12] X. Duan, J. Zhang, Z. Zhu, Y. Liu, Z. Zhang, I. Žutić, and T. Zhou, Antiferroelectric altermagnets: Antiferroelectricity alters magnets, Phys. Rev. Lett. **134**, 106801 (2025).

[13] Z. Zhu, X. Duan, J. Zhang, B. Hao, I. Žutić, and T. Zhou, Two-dimensional ferroelectric altermagnets: From model to material realization, Nano Lett. **25**, 9456 (2025).

[14] F. Zhang *et al.*, Crystal-symmetry-paired spin–valley locking in a layered room-temperature metallic altermagnet candidate, Nat. Phys. **21**, 760 (2025).

[15] O. J. Amin *et al.*, Nanoscale imaging and control of altermagnetism in MnTe, Nature (London) **636**, 348 (2024).

[16] R. D. Gonzalez Betancourt, J. Zubáč, K. Geishendorf, P. Ritzinger, B. Růžičková, T. Kotte, J. Železný, K. Olejník, G. Springholz, B. Büchner, A. Thomas, K. Výborný, T. Jungwirth, H. Reichlová, and D. Kriegner, Anisotropic magnetoresistance in altermagnetic MnTe, npj Spintron. **2**, 45 (2024).

[17] S. Lee, S. Lee, S. Jung, J. Jung, D. Kim, Y. Lee, B. Seok, J. Kim, B. G. Park, L. Šmejkal, C.-J. Kang, and C. Kim, Broken Kramers degeneracy in altermagnetic MnTe, Phys. Rev. Lett. **132**, 036702 (2024).

[18] S. Reimers, L. Odenbreit, L. Šmejkal, V. N. Strocov, P. Constantinou, A. B. Hellenes, R. Jaeschke Ubiergo, W. H. Campos, V. K. Bharadwaj, A. Chakraborty, T. Denneulin, W. Shi, R. E. Dunin-Borkowski, S. Das, M. Kläui, J. Sinova, and M. Jourdan, Direct observation of altermagnetic band splitting in CrSb thin films, Nat. Commun. **15**, 2116 (2024).

[19] Z. Zhou, X. Cheng, M. Hu, R. Chu, H. Bai, L. Han, J. Liu, F. Pan, and C. Song, Manipulation of the altermagnetic order in CrSb via crystal symmetry, Nature (London) **638**, 645 (2025).

[20] G. Yang *et al.*, Three-dimensional mapping of the altermagnetic spin splitting in CrSb, Nat. Commun. **16**, 1442 (2025).

[21] M. Leiviskä, J. Rial, A. Bad'ura, R. L. Seeger, I. Kounta, S. Beckert, D. Kriegner, I. Joumard, E. Schmoranzerová, J. Sinova, O. Gomonay, A. Thomas, Sebastian T. B. Goennenwein, H. Reichlová, L. Š Šmejkal, L. Michez, T. Jungwirth, and V. Baltz, Anisotropy of the anomalous Hall effect in thin films of the altermagnet candidate Mn_5Si_3, Phys. Rev. B **109**, 224430 (2024).

[22] A. Badura *et al.*, Observation of the anomalous Nernst effect in altermagnetic candidate Mn_5Si_3, Nat. Commun. **16**, 7111 (2025).

[23] B. Jiang *et al.*, A metallic room-temperature d-wave altermagnet, Nat. Phys. **21**, 754 (2025).

[24] Z. Wang, S. Yu, X. Cheng, X. Xiao, W. Ma, F. Quan, H. Song, K. Zhang, Y. Zhang, Y. Ma, W. Liu, P. Yadav, X. Shi, Z. Wang, Q. Niu, Y. Gao, B. Xiang, J. Liu, Z. Wang, and X. Chen, Atomic-scale spin sensing of a 2D d-wave altermagnet via helical tunneling, arXiv:2512.23290.

[25] T. Sato, S. Haddad, I. C. Fulga, F. F. Assaad, and J. van den Brink, Altermagnetic anomalous Hall effect emerging from electronic correlations, Phys. Rev. Lett. **133**, 086503 (2024).

[26] B. Brekke, P. Sukhachov, H. G. Giil, A. Brataas, and J. Linder, Minimal models and transport properties of unconventional p-wave magnets, Phys. Rev. Lett. **133**, 236703 (2024).

[27] Z. Jin, Z. Zeng, Y. Cao, and P. Yan, Skyrmion Hall effect in altermagnets, Phys. Rev. Lett. **133**, 196701 (2024).

[28] D.-F. Shao, S.-H. Zhang, M. Li, C.-B. Eom, and E. Y. Tsymbal, Spin-neutral currents for spintronics, Nat. Commun. **12**, 7061 (2021).

[29] Libor Šmejkal, A. B. Hellenes, R. González-Hernández, J. Sinova, and T. Jungwirth, Giant and tunneling magnetoresistance in unconventional collinear antiferromagnets with nonrelativistic spin-momentum coupling, Phys. Rev. X **12**, 011028 (2022).

[30] H. Reichlova *et al.*, Observation of a spontaneous anomalous Hall response in the Mn_5Si_3 d-wave altermagnet candidate, Nat. Commun. **15**, 4961 (2024).

[31] H.-J. Lin, S.-B. Zhang, H.-Z. Lu, and X. C. Xie, Coulomb drag in altermagnets, Phys. Rev. Lett. **134**, 136301 (2025).

[32] J. A. Ouassou, A. Brataas, and J. Linder, dc Josephson effect in altermagnets, Phys. Rev. Lett. **131**, 076003 (2023).

[33] Z. Zhu, R. Huang, X. Chen, Z. Cui, X. Duan, J. Zhang, I. Žutić, and T. Zhou, Altermagnetic proximity effect, Phys. Rev. Lett. **136**, 186702 (2026).

[34] Z. Zhu, X. Chen, X. Duan, Z. Cui, J. Zhang, I. Zutic, and T. Zhou, Altermagnetoelectric spin field effect transistor, arXiv:2512.02974.

[35] Y.-X. Li and C.-C. Liu, Majorana corner modes and tunable patterns in an altermagnet heterostructure, Phys. Rev. B **108**, 205410 (2023).

[36] S. A. A. Ghorashi, T. L. Hughes, and J. Cano, Altermagnetic routes to Majorana modes in zero net magnetization, Phys. Rev. Lett. **133**, 106601 (2024).

[37] Y.-X. Li, Y. Liu, and C.-C. Liu, Creation and manipulation of higher-order topological states by altermagnets, Phys. Rev. B **109**, L201109 (2024).

[38] Y.-X. Li, Realizing tunable higher-order topological superconductors with altermagnets, Phys. Rev. B **109**, 224502 (2024).

[39] Y.-Y. Li and S.-B. Zhang, Floating edge bands in the Bernevig-Hughes-Zhang model with altermagnetism, Phys. Rev. B **111**, 045106 (2025).

[40] X. Huo, X. Zhu, C.-A. Li, S. Feng, S.-B. Zhang, S. A. Yang, and H. Guo, Altermagnetism and its induced higher-order topology on the Lieb lattice, Phys. Rev. B **113**, 024420 (2026).

[41] M. S. Rudner and L. S. Levitov, Topological transition in a non-Hermitian quantum walk, Phys. Rev. Lett. **102**, 065703 (2009).

[42] Y. C. Hu and T. L. Hughes, Absence of topological insulator phases in non-Hermitian *PT*-symmetric Hamiltonians, Phys. Rev. B **84**, 153101 (2011).

[43] T. E. Lee, Anomalous edge state in a non-Hermitian lattice, Phys. Rev. Lett. **116**, 133903 (2016).

[44] H. Shen, B. Zhen, and L. Fu, Topological band theory for non-Hermitian Hamiltonians, Phys. Rev. Lett. **120**, 146402 (2018).

[45] S. Yao and Z. Wang, Edge states and topological invariants of non-Hermitian systems, Phys. Rev. Lett. **121**, 086803 (2018).

[46] S. Yao, F. Song, and Z. Wang, Non-Hermitian Chern bands, Phys. Rev. Lett. **121**, 136802 (2018).

[47] F. K. Kunst, E. Edvardsson, J. C. Budich, and E. J. Bergholtz, Biorthogonal bulk-boundary correspondence in non-Hermitian systems, Phys. Rev. Lett. **121**, 026808 (2018).

[48] T. T. Koutserimpas and R. Fleury, Nonreciprocal gain in non-Hermitian time-Floquet systems, Phys. Rev. Lett. **120**, 087401 (2018).

[49] S. Longhi, Topological phase transition in non-Hermitian quasicrystals, Phys. Rev. Lett. **122**, 237601 (2019).

[50] T. Liu, Y.-R. Zhang, Q. Ai, Z. Gong, K. Kawabata, M. Ueda, and F. Nori, Second-order topological phases in non-Hermitian systems, Phys. Rev. Lett. **122**, 076801 (2019).

[51] X.-W. Luo and C. Zhang, Higher-order topological corner states induced by gain and loss, Phys. Rev. Lett. **123**, 073601 (2019).

[52] N. Matsumoto, K. Kawabata, Y. Ashida, S. Furukawa, and M. Ueda, Continuous phase transition without gap closing in non-Hermitian quantum many-body systems, Phys. Rev. Lett. **125**, 260601 (2020).

[53] L. Xiao, T. Deng, K. Wang, G. Zhu, Z. Wang, W. Yi, and P. Xue, Non-Hermitian bulk–boundary correspondence in quantum dynamics, Nat. Phys. **16**, 761 (2020).

[54] E. J. Bergholtz, J. C. Budich, and F. K. Kunst, Exceptional topology of non-Hermitian systems, Rev. Mod. Phys. **93**, 015005 (2021).

[55] K. Ding, C. Fang, and G. Ma, Non-Hermitian topology and exceptional-point geometries, Nat. Rev. Phys. **4**, 745 (2022).

[56] Y. Li, X. Ji, Y. Chen, X. Yan, and X. Yang, Topological energy braiding of non-Bloch bands, Phys. Rev. B **106**, 195425 (2022).

[57] X. Zhang, T. Zhang, M.-H. Lu, and Y.-F. Chen, A review on non-Hermitian skin effect, Adv. Phys.: X **7**, 2109431 (2022).

[58] S. Weidemann, M. Kremer, S. Longhi, and A. Szameit, Topological triple phase transition in non-Hermitian Floquet quasicrystals, Nature (London) **601**, 354 (2022).

[59] N. Okuma and M. Sato, Non-Hermitian topological phenomena: A review, Annu. Rev. Condens. Matter Phys. **14**, 83 (2023).

[60] X. Ji and X. Yang, Generalized bulk-boundary correspondence in periodically driven non-Hermitian systems, J. Phys.: Condens. Matter **36**, 243001 (2024).

[61] B.-B. Wang, Z. Cheng, H.-Y. Zou, Y. Ge, K.-Q. Zhao, Q.-R. Si, S.-Q. Yuan, H.-X. Sun, H. Xue, and B. Zhang, Observation of disorder-induced boundary localization, Proc. Natl. Acad. Sci. USA **122**, e2422154122 (2025).

[62] X. Ji, H. Geng, N. Akhtar, and X. Yang, Floquet engineering of point-gapped topological superconductors, Phys. Rev. B **111**, 195419 (2025).

[63] C. M. Bender and S. Boettcher, Real spectra in non-Hermitian Hamiltonians having $\mathcal{PT}$ symmetry, Phys. Rev. Lett. **80**, 5243 (1998).

[64] H. Hodaei, A. U. Hassan, S. Wittek, H. Garcia-Gracia, R. El-Ganainy, D. N. Christodoulides, and M. Khajavikhan, Enhanced sensitivity at higher-order exceptional points, Nature (London) **548**, 187 (2017).

[65] Y. Ashida, Z. Gong, and M. Ueda, Non-Hermitian physics, Adv. Phys. **69**, 249 (2020).

[66] R. Lin, T. Tai, M. Yang, L. Li, and C. H. Lee, Topological non-Hermitian skin effect, Front. Phys. **18**, 53605 (2023).

[67] H. Wang, J. Zhong, and S. Fan, Non-Hermitian photonic band winding and skin effects: A tutorial, Adv. Opt. Photonics **16**, 659 (2024).

[68] X. Yang, Y. Feng, A. Wahab, and H. Geng, Non-Hermitian second-order topological phases and bipolar skin effect in photonic kagome crystals, Phys. Rev. A **113**, 023506 (2026).

[69] M.-A. Miri and A. Alù, Exceptional points in optics and photonics, Science **363**, eaar7709 (2019).

[70] S.-X. Wang and Z. Yan, Theory for the spectral splitting exponent of exceptional points, Phys. Rev. B **112**, 195125 (2025).

[71] V. M. Matinez Alvarez, J. E. Barrios Vargas, and L. E. F. Foa Torres, Non-Hermitian robust edge states in one dimension: Anomalous localization and eigenspace condensation at exceptional points, Phys. Rev. B **97**, 121401(R) (2018).

[72] F. Song, S. Yao, and Z. Wang, Non-Hermitian topological invariants in real space, Phys. Rev. Lett. **123**, 246801 (2019).

[73] F. Song, S. Yao, and Z. Wang, Non-Hermitian skin effect and chiral damping in open quantum systems, Phys. Rev. Lett. **123**, 170401 (2019).

[74] K. Zhang, Z. Yang, and C. Fang, Correspondence between winding numbers and skin modes in non-Hermitian systems, Phys. Rev. Lett. **125**, 126402 (2020).

[75] N. Okuma, K. Kawabata, K. Shiozaki, and M. Sato, Topological origin of non-Hermitian skin effects, Phys. Rev. Lett. **124**, 086801 (2020).

[76] L. Li, C. H. Lee, S. Mu, and J. Gong, Critical non-Hermitian skin effect, Nat. Commun. **11**, 5491 (2020).

[77] K. Zhang, Z. Yang, and C. Fang, Universal non-Hermitian skin effect in two and higher dimensions, Nat. Commun. **13**, 2496 (2022).

[78] S. Manna and B. Roy, Inner skin effects on non-Hermitian topological fractals, Commun. Phys. **6**, 10 (2023).

[79] B. Hetényi and B. Dóra, Localized states and skin effect around non-Hermitian impurities in tight-binding models, Phys. Rev. B **112**, 075123 (2025).

[80] T. Yoshida, S.-B. Zhang, T. Neupert, and N. Kawakami, Non-Hermitian Mott skin effect, Phys. Rev. Lett. **133**, 076502 (2024).

[81] E. Zhao, Z. Wang, C. He, T. F. J. Poon, K. K. Pak, Y.-J. Liu, P. Ren, X.-J. Liu, and G.-B. Jo, Two-dimensional non-Hermitian skin effect in an ultracold Fermi gas, Nature (London) **637**, 565 (2025).

[82] C. H. Lee, L. Li, and J. Gong, Hybrid higher-order skin-topological modes in nonreciprocal systems, Phys. Rev. Lett. **123**, 016805 (2019).

[83] L. Li, C. H. Lee, and J. Gong, Topological switch for non-Hermitian skin effect in cold-atom systems with loss, Phys. Rev. Lett. **124**, 250402 (2020).

[84] K. Kawabata, M. Sato, and K. Shiozaki, Higher-order non-Hermitian skin effect, Phys. Rev. B **102**, 205118 (2020).

[85] D. Zou, T. Chen, W. He, J. Bao, C. H. Lee, H. Sun, and X. Zhang, Observation of hybrid higher-order skin-topological effect in non-Hermitian topolectrical circuits, Nat. Commun. **12**, 7201 (2021).

[86] Y. Fu, J. Hu, and S. Wan, Non-Hermitian second-order skin and topological modes, Phys. Rev. B **103**, 045420 (2021).

[87] W. Zhu and J. Gong, Hybrid skin-topological modes without asymmetric couplings, Phys. Rev. B **106**, 035425 (2022).

[88] Y. Li, C. Liang, C. Wang, C. Lu, and Y.-C. Liu, Gain-loss-induced hybrid skin-topological effect, Phys. Rev. Lett. **128**, 223903 (2022).

[89] J. Sun, C.-A. Li, S. Feng, and H. Guo, Hybrid higher-order skin-topological effect in hyperbolic lattices, Phys. Rev. B **108**, 075122 (2023).

[90] Y. Sun, X. Hou, T. Wan, F. Wang, S. Zhu, Z. Ruan, and Z. Yang, Photonic Floquet skin-topological effect, Phys. Rev. Lett. **132**, 063804 (2024).

[91] X. Ji, W. Ding, Y. Chen, and X. Yang, Non-Hermitian second-order topological superconductors, Phys. Rev. B **109**, 125420 (2024).

[92] W. Zhu and L. Li, A brief review of hybrid skin-topological effect, J. Phys.: Condens. Matter **36**, 253003 (2024).

[93] M. Lu, X.-X. Zhang, and M. Franz, Magnetic suppression of non-Hermitian skin effects, Phys. Rev. Lett. **127**, 256402 (2021).

[94] H. T. Teo, S. Mandal, Y. Long, H. Xue, and B. Zhang, Pseudomagnetic suppression of non-Hermitian skin effect, Sci. Bull. **69**, 1667 (2024).

[95] G. K. Dash, S. Panda, and S. Nandy, Fingerprint of non-Hermiticity in a d-wave altermagnet, Phys. Rev. B **111**, 155119 (2025).

[96] M. A. Reja and A. Narayan, Emergence of tunable exceptional points in altermagnet-ferromagnet junctions, Phys. Rev. B **110**, 235401 (2024).

[97] B. A. Bernevig, T. L. Hughes, and S.-C. Zhang, Quantum spin Hall effect and topological phase transition in HgTe quantum wells, Science **314**, 1757 (2006).

[98] Z. Yan, Majorana corner and hinge modes in second-order topological insulator/superconductor heterostructures, Phys. Rev. B **100**, 205406 (2019).

[99] X. Qian, J. Liu, L. Fu, and J. Li, Quantum spin Hall effect in two-dimensional transition metal dichalcogenides, Science **346**, 1344 (2014).

[100] S. Longhi, Erratic non-Hermitian skin localization, Phys. Rev. Lett. **134**, 196302 (2025).

[101] Q. Liang, D. Xie, Z. Dong, H. Li, H. Li, B. Gadway, W. Yi, and B. Yan, Dynamic signatures of non-Hermitian skin effect and topology in ultracold atoms, Phys. Rev. Lett. **129**, 070401 (2022).

[102] W. Zhu, X. Fang, D. Li, Y. Sun, Y. Li, Y. Jing, and H. Chen, Simultaneous observation of a topological edge state and exceptional point in an open and non-Hermitian acoustic system, Phys. Rev. Lett. **121**, 124501 (2018).

[103] T. Helbig, T. Hofmann, S. Imhof, M. Abdelghany, T. Kiessling, L. W. Molenkamp, C. H. Lee, A. Szameit, M. Greiter, and R. Thomale, Generalized bulk–boundary correspondence in non-Hermitian topolectrical circuits, Nat. Phys. **16**, 747 (2020).

[104] H. Geng, J. Y. Wei, M. H. Zou, L. Sheng, W. Chen, and D. Y. Xing, Nonreciprocal charge and spin transport induced by non-Hermitian skin effect in mesoscopic heterojunctions, Phys. Rev. B **107**, 035306 (2023).
[105] K. Shao, H. Geng, E. Liu, J. L. Lado, W. Chen, and D. Y. Xing, Non-Hermitian moiré valley filter, Phys. Rev. Lett. **132**, 156301 (2024).
[106] M. Wu, M. Weng, Z. Chi, S. Zheng, F. Liu, C. Shang, B. Zhang, Q. Zhao, Y. Meng, and J. Zhou, Gain-and-loss-free metamaterials exhibiting non-Hermitian non-Bloch effects, Phys. Rev. Lett. **136**, 106603 (2026).
[107] T. Hu, W. Zhong, T. Zhang, W. Wang, and Z. F. Wang, Identifying topological corner states in two-dimensional metal-organic frameworks, Nat. Commun. **14**, 7092 (2023).
[108] T. Zhang, S. Vlaic, S. Pons, D. Roditchev, V. Sheina, C. David, G. Rodary, J.-C. Girard, and H. Aubin, Scanning tunneling microscopy observation of the hinge states of bismuth nanocrystals, Phys. Rev. B **108**, 085422 (2023).